Redox Biology 11 (2017) 231–239

Contents lists available at ScienceDirect

Redox Biology

journal homepage: www.elsevier.com/locate/redox

Research Paper

On the nature of the Cu-rich aggregates in brain astrocytes

Brendan Sullivan[a], Gregory Robison[a,1], Jenna Osborn[a,2], Martin Kay[a], Peter Thompson[a], Katherine Davis[a,3], Taisiya Zakharova[a], Olga Antipova[b,c], Yulia Pushkar[a,*]

[a] Department of Physics and Astronomy, Purdue University, 525 Northwestern Ave., West Lafayette, IN 47907, United States
[b] BioCAT, Advanced Photon Source, Argonne National Laboratory, 9700 S. Cass Ave., Argonne, IL 60439, United States
[c] XSD, Argonne National Laboratory, 9700 S. Cass Ave., Argonne, IL 60439, United States

ARTICLE INFO

Keywords:
X-ray fluorescence microscopy
Subventricular zone
Cu
Metallothionein

ABSTRACT

Fulfilling a bevy of biological roles, copper is an essential metal for healthy brain function. Cu dyshomeostasis has been demonstrated to be involved in some neurological conditions including Menkes and Alzheimer's diseases. We have previously reported localized Cu-rich aggregates in astrocytes of the subventricular zone (SVZ) in rodent brains with Cu concentrations in the hundreds of millimolar. Metallothionein, a cysteine-rich protein critical to metal homeostasis and known to participate in a variety of neuroprotective and neuroregenerative processes, was proposed as a binding protein. Here, we present an analysis of metallothionein(1,2) knockout (MTKO) mice and age-matched controls using X-ray fluorescence microscopy. In large structures such as the corpus callosum, cortex, and striatum, there is no significant difference in Cu, Fe, or Zn concentrations in MTKO mice compared to age-matched controls. In the astrocyte-rich subventricular zone where Cu-rich aggregates reside, approximately 1/3 as many Cu-rich aggregates persist in MTKO mice resulting in a decrease in periventricular Cu concentration. Aggregates in both wild-type and MTKO mice show XANES spectra characteristic of Cu_xS_y multimetallic clusters and have similar [S]/[Cu] ratios. Consistent with assignment as a Cu_xS_y multimetallic cluster, the astrocyte-rich SVZ of both MTKO and wild-type mice exhibit autofluorescent bodies, though MTKO mice exhibit fewer. Furthermore, XRF imaging of Au-labeled lysosomes and ubiquitin demonstrates a lack of co-localization with Cu-rich aggregates suggesting they are not involved in a degradation pathway. Overall, these data suggest that Cu in aggregates is bound by either metallothionein-3 or a yet unknown protein similar to metallothionein.

1. Introduction

Owing to the brain's extreme metabolic demands and the wide range of biochemistry facilitated by copper (Cu), significant amounts of Cu are involved in the brain's function [13]. Serving as a cofactor of key proteins involved in mitochondrial activity, neurotransmitter and neuropeptide biosynthesis, oxidative stress defense and other critical brain processes, Cu is essential for normal brain function [50,64]. Redox active copper cycles between the cuprous (I) and cupric (II) forms to accomplish catalytic functions in proteins. Elevated Cu concentration has been noted in synaptic vesicles and its release during synaptic transmission has been suggested to play a role in synaptic plasticity and long-term potentiation [19,23]. Cu ions can also be damaging for the organism if they participate in reactions which generate oxidative stress. Since free Cu ions are toxic to the cell, sophisticated Cu transport and Cu chaperone systems have developed which involve proteins with extremely high Cu affinities [21]. Studies in yeast have found on average less than one free Cu ion per cell [55]. It is not surprising that perturbations to Cu homeostasis have been implicated in a number of devastating neurodegenerative diseases. Menkes and Wilson's diseases, for instance, have been shown to be manifestations of Cu deficiency and Cu overload caused by mutations in the copper transporting proteins ATP7A and ATP7B, respectively [12,72]. Additionally, there is an extensive body of literature implicating metal dyshomeostasis – in particular Cu and Zn - with the formation of plaques in the brain during neurodegeneration [22,3,40].

We demonstrated Cu-rich aggregates in glial fibrillary acid protein-positive (GFAP+) astrocytes in the subventricular zone [52,53] and other brain areas such as the hippocampus and rostral migratory steam of rats [66]. Further characterization of Cu rich aggregates showed that

* Corresponding author.
E-mail address: ypushkar@purdue.edu (Y. Pushkar).
[1] Current address: Department of Physics and Astronomy, Hanover College, Hanover IN 47243.
[2] Current address: Department of Biomedical Engineering, Duke University, Durham, NC 27707.
[3] Current address: Department of Chemistry, Princeton University, Princeton NJ 08544.

http://dx.doi.org/10.1016/j.redox.2016.12.007
Received 17 August 2016; Received in revised form 4 November 2016; Accepted 2 December 2016
Available online 09 December 2016
2213-2317/

they are about a micron in diameter and can achieve localized concentrations of hundreds of millimolar [66]. The results on the Cu distribution in rodent brains were later verified by others using XRF [51] and LA-ICP-MS [20,37,6]. In the brain, astrocytes are thought to play a key role in copper homeostasis [57]. Possible pathways for Cu transport into the brain astrocytes include Cu absorption either from the blood or the cerebrospinal fluid (CSF). Astrocytes have perivascular end-feet or foot-plates, expanses of their cytoplasmic processes that surround the abluminal surfaces of the capillary endothelial cells that form the blood brain barrier (BBB) of the brain and are opposed to the endothelial basal lamina [1]. The BBB is partially lost on the surface of blood capillaries in the subventricular zone (SVZ) [67] which can explain the highest Cu accumulations detected in astrocytes positioned close to the ventricle wall [52,53]. Some of the astrocytes in the SVZ retain direct exposure to the surface of the ventricle wall even in adults [38]. Thus, astrocytes have preferential (as compared to neurons) access to the interstitial fluids as well as the CSF. As such, it has been proposed that astrocytes can serve as Cu "depots" for the brain [57,68] by accumulating metal which can later be used by the astrocyte or routed to neurons. Supporting this argument, it is important to note that astrocytes are capable of Cu uptake and export [58,59]. It is commonly believed that glutathione and metallothioneins – a family of metal-binding, cysteine rich proteins – are imperative to astrocytes' ability to buffer Cu [57].

To gain insight into the formation mechanism and biological significance of Cu-rich aggregates, it would be beneficial to determine their protein composition. XRF analysis of the [S]/[Cu] ratio and XANES spectroscopic analysis suggested Cu binding in the form of Cu_xS_y multimetallic cluster. Metallothionein (MT) was identified as a candidate binding protein [53]. Thus, we sought to characterize the metal distribution in a MT(1,2) knockout (MTKO) mouse in combination with other biological markers. Note that MT has three isoforms present in the central nervous system (CNS). MT1 and MT2 are regulated and produced coordinately, and are often described together as one functional entity. They are present primarily in GFAP+ glial cells in the brain [42,43,75] while MT3 is present in both astrocytes and neurons [28,74]. The MTKO mouse, which contains a disruption vector at the MT1 and MT2 genes, was originally reported to have increased sensitivity to transition metal toxicity, especially Cd, and poorer mitigation of oxidative stress [18,36,73]. Further studies on the MTKO phenotype in the brain have also implicated metallothionein in inducing reactive gliosis [34] and aiding in recovery from brain injury [17,48,70].

Using XRF, we report spatial quantification of biologically relevant metal ions in the brains of MTKO mice as compared to age-matched wild type (WT) mice. It is demonstrated that MTKO mice possess Cu-rich aggregates in the SVZ. The absence of MT(1,2), however, results in fewer aggregates in the SVZ though the remaining aggregates exhibit similar Cu concentrations in both MTKO and WT mice. Cu-rich aggregates in MTKO mice brains, however, exhibit similar [S]/[Cu] ratios and XANES spectra as WT mice, suggesting Cu is bound in similar Cu_xS_y multimetallic clusters. According to previous literature Cu_xS_y clusters formed with biomolecules display autofluorescence [45]. We indeed find that GFAP+ cells in the SVZ show autofluorescence following UV (350 nm) excitation. Autofluorescing bodies are similar in shape and size to the detected Cu-rich aggregates. Overall the data strongly suggest that Cu in Cu-rich aggregates is bound to metallothionein or a protein similar to metallothionein. Similarly, the data demonstrate that metallothionein plays a role in their formation with MT3 likely fulfilling the role of metallothionein(1,2) in MTKO mice.

2. Materials and methods

2.1. Animals

Male Sprague-Dawley rats were purchased from Harlan (Indianapolis). Male 129S1/SvImJ (wild type) and 129S7/SvEvBrd-$MT1^{tm1Bri}MT2^{tm1Bri}$ mice (MTKO), an MT(1,2) double knockout mouse) were purchased from Jackson Labs [36]. Rats were sacrificed at 12 weeks old. Mice were sacrificed at 3 or 9 weeks old, as specified in the text. Immediately following extraction, the whole brain was snap frozen on liquid nitrogen and stored at −80 °C until sectioning. All experiments complied with animal rights regulations and were approved by the Institutional Committee on Animal Use at Purdue University.

2.2. Preparation of brain sections

Frozen sections were prepared in a Shandon FE/SE cryomicrotome (Thermo Scientific). To prevent sample contamination, Teflon coated blades were used. Samples were not fixed or chemically treated in any way. After being cut, sections containing the lateral ventricle (bregma=−0.8 mm) were placed on either glass microscope slides for conventional microscopy or X-ray compatible substrates made of 4 μm thick polypropylene film stretched flat on a frame for XRF microscopy. Sample thickness was either 30 μm (XRF, 8-BM, 18-ID), 10 μm (optical microscopy, XRF 2-ID-D/E and 20-ID). Samples were stored at −80 °C prior to use.

2.3. Synchrotron based X-ray fluorescence (XRF) microscopy

Elemental mapping was performed at the Advanced Photon Source (APS). A description of the BioCAT microprobe (beamline 18-ID) beamline is available at [4], a description of the x-ray microprobe (2-ID-D) at [15]. For imaging parameters used in the presented data, see Table 1. Focusing was done by KB mirrors (8-BM, 18-ID, and 20-ID) or Fresnel zone plates (2-ID-D/E) to the spot size specified in Table 1. The fluorescence spectra were recorded by an energy resolving silicon drift detector and fitted used the program MAPS [71]. Spectra are normalized by incident flux as measured by an ionization chamber. Quantitation was carried out using the NIST thin film standards NBS-1832 and NBS-1833 [46] or the AXO thin film XRF standard (AXO GmbH, Dresden).

Table 1
X-ray fluorescence microcopy imaging parameters.

Figure	Beamline	Pixel size μm^2 (v)×(h)	Beam size μm^2 (v)×(h)	Dwell time (sec)	Flux (photons/s)	X-ray energy (keV)
1A,Table 2(3 week)	**18-ID**	**20×20**	**5×5**	**0.05–0.20**	**2×10^{13}**	**10.0**
Table 2 (9 week)	**8-BM-B**	**25×25**	**25×25**	**0.25**	**4×10^{10}**	**10.0**
1B,Table 3	**18-ID**	**5×5**	**5×5**	**0.05–0.20**	**2×10^{13}**	**10.0**
1C,Table 4	**2-ID-D**	**0.3×0.3**	**0.2×0.25**	**1.0**	**4×10^{9}**	**10.0**
2, Inset	**20-ID-B**	**10×10**	**7×7**	**0.2**	**2×10^{12}**	**10.0**
2, Spectra	**20-ID-B**	**n/a**	**7×7**	**1–2**	**2×10^{12}**	**8.88–9.22**
4B	**2-ID-D**	**0.3×0.3**	**0.3×0.3**	**3.0**	**4×10^{8}**	**13.0**
4E	**2-ID-E**	**0.3×0.3**	**0.3×0.3**	**1.5**	**4×10^{8}**	**12.7**

Table 2
Quantitation from 25×25 μm^2 scans (n =3 per group).

	Fe (μg/g)		Cu (μg/g)		Zn (μg/g)	
3 Week	**MTKO**	**WT**	**MTKO**	**WT**	**MTKO**	**WT**
Corpus callosum	11.24 ± 1.34	9.64 ± 0.22	2.21 ± 0.29	2.08 ± 0.17	13.45 ± 1.53	12.52 ± 0.26
Cortex	15.92 ± 1.98	13.73 ± 0.12	3.15 ± 0.43	2.66 ± 0.12	17.94 ± 2.06	16.07 ± 0.29
Striatum	17.06 ± 2.18	13.61 ± 0.46	3.11 ± 0.43	2.59 ± 0.12	18.26 ± 2.41	16.53 ± 0.46
SVZ	18.51 ± 3.25	23.03 ± 1.81	6.87 ± 0.51	9.60 ± 0.57	15.38 ± 1.40	16.66 ± 0.53
9 Week						
Corpus Callosum	9.66 ± 1.19	8.00 ± 1.01	3.78 ± 0.26	3.61 ± 0.34	10.14 ± 0.12	9.79 ± 0.77
Cortex	11.02 ± 0.62	12.51 ± 1.71	4.12 ± 0.19	3.98 ± 0.44	12.59 ± 0.24	12.66 ± 1.22
Striatum	12.15 ± 0.13	11.72 ± 1.66	4.23 ± 0.14	3.86 ± 0.24	13.10 ± 0.30	12.97 ± 1.05
SVZ	24.74 ± 18.51	30.51 ± 27.82	9.85 ± 2.15	10.71 ± 0.84	13.60 ± 1.27	13.32 ± 1.07

Table 3
Quantitation of 5×5 μm^2 SVZ scans (n =3 per group; 3-week old mice).

	MTKO	WT
Fe (μg/g)	38.08 ± 5.44[§]	37.81 ± 9.49
Cu (μg/g)[*]	15.94 ± 0.56	22.56 ± 2.04
Zn (μg/g)	22.65 ± 3.95	23.47 ± 4.45

[*] $p < 0.05$.
[§] One sample, which was ruled to be an outlier by Grubb's test at $p < 0.05$, was excluded from calculating the Fe mean as it contained blood which is Fe-rich. No differences were detected in Cu or Zn.

Table 4
Comparison of aggregates in MTKO and WT mice (n=2 3-week old animals per group, > 10 aggregates per animal).

	MTKO		WT	
Cu threshold (μg/g)	**< 60 μg/g**	**> 60 μg/g**	**< 60 μg/g**	**> 60 μg/g**
[Fe] (μg/g)	49.35 ± 9.15	70.23 ± 22.11	27.85 ± 8.74	43.18 ± 9.45
[Cu] (μg/g)	11.03 ± 0.58[**]	519.85 ± 136.47	24.85 ± 0.60	514.76 ± 57.16
[Zn] (μg/g)	21.56 ± 4.21	23.31 ± 0.21	19.82 ± 0.66	24.19 ± 1.76
[S]/[Cu][‡]	5.36 ± 0.10[*]	1.18 ± 0.11	4.26 ± 0.08	1.09 ± 0.02
Aggregate density (aggregates/μm)[‡]	n/a	0.06 ± 0.02	n/a	0.16 ± 0.05

[*] $p < 0.05$,
[**] $p < 0.01$ between MTKO and WT at the same threshold level
[‡] $p < 0.01$ between different threshold levels

2.4. Quantitation of Cu hotspots

For XRF images recorded with tissue level resolution (5 and 20 μm), regions of interest were determined by comparison with a brain atlas (20 μm resolution, Table 2) or by selecting pixels with a Cu concentration greater than 12 μg/g which served to define a region of interest for the SVZ (5 μm, Table 3,Fig. S2). From these regions, the average metal content is readily determined (Tables 2, 3). For higher resolution images (300–500 nm), XRF maps were analyzed based on a static threshold of 60 μg/g. Pixels below 60 μg/g reflect the basal level of Cu in the SVZ while pixels above 60 μg/g reliably isolate aggregates (Fig. S3). Quantitation of these regions are given in Table 4. Note that while changing the threshold used to determine regions of interest will change mean concentrations, all reported significances do not change around the reported thresholds (minimum ± 5 μg/g) and results agree with quantitation of hand-drawn regions of interest (data now shown).

2.5. Micro-cryo-XANES from tissue sections

10 μm thick coronal sections from both WT and MTKO mice were placed in a Linkam BCS196 cryostage modified to be compatible with X-ray measurements and kept at −100 °C to mitigate X-ray damage. An elemental map was first recorded from which spots to record XANES were determined. For these scans, dwell times were limited to less than 2 s which is considerably less than the time of a XANES scan. The monochromator was calibrated by setting the inflection point of a Cu foil reference to be 8980.0 eV. The stability of this energy calibration was ensured by simultaneously recording the reference Cu foil with samples. Damage studies were conducted and no shift in the edge location was detected in more than four scans per spot. The data presented here are summed from 114 wild type spectra recorded from 28 spots and 28 MTKO spectra recorded from 14 spots.

2.6. Immunohistochemical staining

Frozen (−80 °C) brain sections on microscope slides or on 4 μm polypropylene film were thawed, fixed with 4% paraformaldehyde (PFA) in phosphate buffered saline (PBS) for 5 (GFAP, UBQ, MT(1,2)), 15 (Ki67, LAMP1) minutes at room temperature (RT), washed twice with PBS, treated for 1 h at RT sequentially with: 1) blocking/ permeabilization solution: (2% (w/v) bovine serum albumin (BSA) /0.2% (v/v) Triton X-100 in PBS), 2) primary antibodies in PBS containing 2% BSA at dilutions specified in the antibodies listing, 3) secondary antibodies in PBS containing 2% BSA as specified in the antibodies section. Three, five minute washes with PBS were performed after treatment with primary and secondary antibodies. Sections on microscope slides were subjected to ProLong Gold antifade reagent before being covered with a coverslip. Slides were sealed and stored at 4 °C. Sections on 4 μm polypropylene film were XRF imaged immediately after staining and very quick rinse with distilled, deionized (18 MΩ) water to remove excess phosphorous from PBS. Treatments of brain tissue during staining result in partial Cu loss and increased Cu background in XRF maps in the tissue as compared to fresh, untreated sections.

2.7. Antibodies

The following antibodies were used in the following concentrations (v/v with 2% BSA in PBS): rabbit polycloncal anti-Ki67 (abcam ab155580, 1:300), rabbit polyclonal anti-GFAP (Thermo-Fisher 180063, 1:500), mouse monoclonal anti-GFAP (Millipore MAB360), rabbit polycloncal anti-LAMP1 (abcam ab24170, 1:300), rabbit polyclonal anti-ubiquitin (abcam ab7780, 1:50), mouse monoclonal anti-MT(1,2) (abcam ab12228, 1:50), goat anti-rabbit Alexafluor 488 (Thermo-Fisher A-110066, 1:1000), goat anti-mouse AlexaFluor 488 (Thermo-Fisher A-11001, 1:1000), goat anti-rabbit 1.4 nm Au nanoconjugates (Nanoprobes #2003, 1:50).

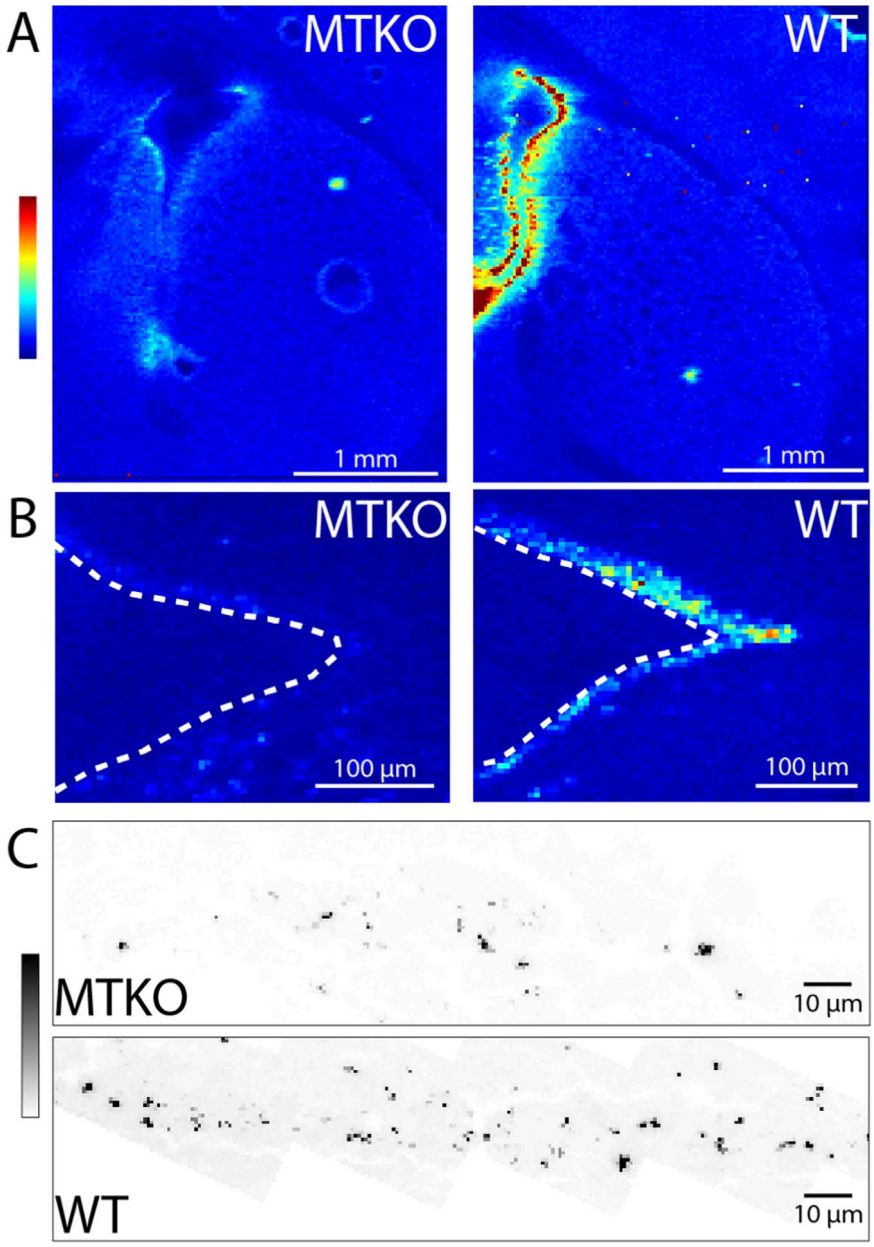

Fig. 1. Comparison of MTKO and wild type Cu concentrations. **A.** Tissue level Cu maps with 25 µm resolution. **B.** Cu XRF maps of the SVZ with 5 µm resolution. **C.** Cu XRF maps of the SVZ with 300 nm resolution. These data are from 3-week old mice.

2.8. Quantitation of neurogenesis in the SVZ

To quantify neurogenesis, Ki67 stained sections were imaged on an Olympus BX43 upright microscope with a DP-72 camera. As Ki67 is present in the nucleus of actively dividing cells, it was possible to count discrete puncta that represent dividing cells. These were counted by hand and normalized for ventricle length. This normalized cell number (with units of cells/µm) is used to quantify neurogenesis.

2.9. Detection of optical autofluorescence

Autofluorescence from Cu aggregates was detected using a Fast Red filter cube (Chroma, Bellow Falls, VT) which has an excitation filter at 350 nm, and a longpass emission filter at 550 nm. In order to co-localize autofluorescence with immunostaining, the immunostained image was transformed via a similarity transformation to hand-chosen landmarks to match the autofluorescence image [56]. Features for the transformation were chosen by morphological features in the ventricle or choroid plexus (i.e. not fluorescence) and at least 10 were chosen per transformation.

2.10. Statistical analysis

Data are presented as mean ± SEM. For quantitation, the number of rodents is given in appropriate tables. The phrase "n=N per group" means that at least one section from N animals was imaged and used in quantification. For comparison of means, one-way ANOVA was used; statistical significance is taken at $p < 0.05$.

3. Results

3.1. Quantitative XRF imaging of MT (1,2) knockout mice (MTKO)

For quantitative analysis, MTKO knockout mice were XRF imaged at tissue level (20×20 or 25×25 µm^2) resolution and compared with age-matched controls. As MT is involved with Cu and Zn homeostasis

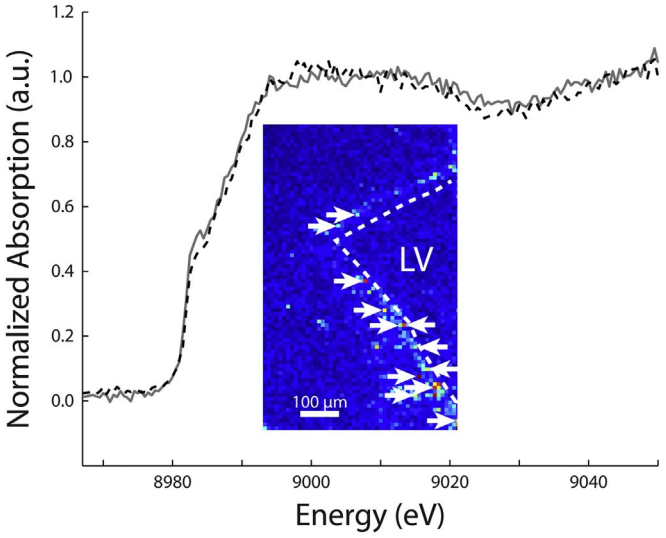

Fig. 2. Summed XANES scans for wild type (gray, solid) and MTKO (black, dashed) rodents recorded directly from tissue. Inset: representative Cu XRF map with arrows pointing to positions from which XANES scans were recorded. Data are from 9-week old mice.

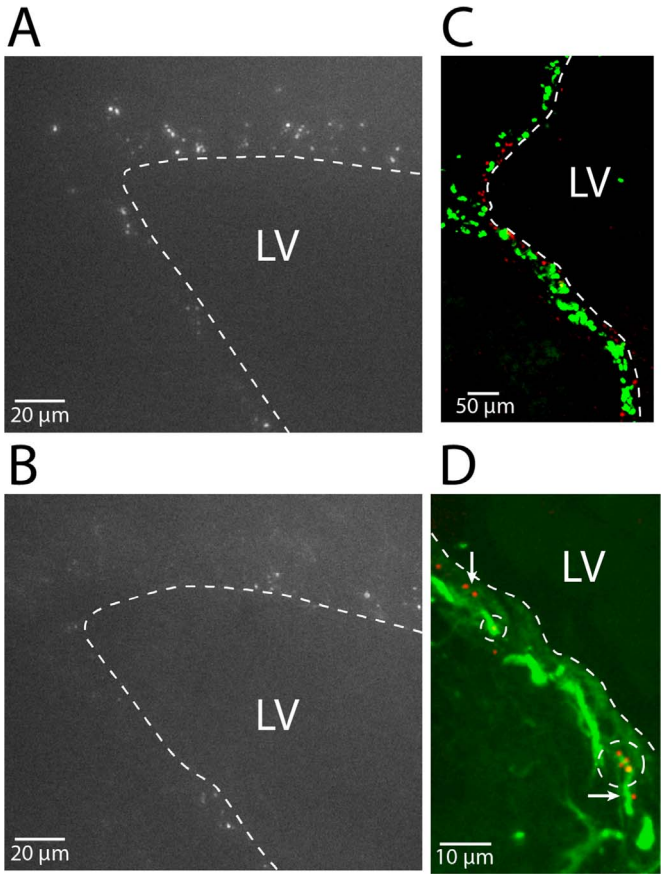

Fig. 3. Representative autofluorescence at the lateral ventricle corner for (**A**) wild-type mice and (**B**) MTKO mice at 40× magnification. **C.** Cu autofluorescence (red) with Ki67 (green) on the same section, showing that Cu does not accumulate in actively dividing cells, consistent with previous findings. **D.** Cu autofluorescence (red) with GFAP (green) in the SVZ demonstrating that periventricular Cu aggregates reside in astrocytes as previously demonstrated. Circles show regions of strong co-localization while arrows show aggregates that likely reside in astrocyte processes. Data are from 9 week old mice. (For interpretation of the references to color in this figure legend, the reader is referred to the web version of this article.)

we checked whether the content of these metals is altered in the brain (Fig. 1A,Table 2,S1). Structures analyzed for differences were the striatum, corpus callosum, cortex, and subventricular zone. XRF did not reveal any statistically significant difference in Cu, Zn or Fe for structures examined. Thus, the overall metal content in the brain is not significantly affected by MT (1,2) knockout, at least at 3 and 9 weeks of age. However, significant differences were detected in the SVZ. This area was analyzed with increased (5 µm) spatial resolution to allow isolation of the SVZ for quantitation (Fig. 1B and S2,Table 3**)**. The SVZ was also imaged with submicron resolution which allows individual aggregates to be visualized for analysis (Fig. 1C and S3,Table 4). While both WT and MTKO mice exhibit a [S]/[Cu] ratio consistent with previously studied Cu aggregates in the rat brain [53], the number of Cu aggregates in MTKO dropped considerably. There were approximately one-third as many aggregates per ventricle length in MTKO mice as compared to wild type mice (Table 4,Fig. 1C). The concentration of Cu in individual Cu aggregates was comparable though basal Cu in the SVZ was decreased in MTKO mice (Table 4).

3.2. Cu-rich aggregates in both wild type and MTKO mice are bound as Cu-S Clusters

To determine if Cu aggregates in MTKO and WT mice were bound as Cu_xS_y clusters as we previously reported for healthy rats, XANES measurements at the Cu K-edge were carried out on Cu aggregates. XANES measurements are uniquely sensitive to the oxidation state and ligand environment of metal ions in biological systems. In cuprous-thiolate clusters, for instance, a major feature appears at ~8983 eV as a result of a 1s→4p transition whose intensity is defined by the Cu coordination environment. Cu(II) ions do not exhibit this feature [31]. This feature has been used previously to characterize not only metallothioneins but a wide variety of Cu_xS_y compounds from biological systems [24,25,49].

A fluorescence map was first recorded along the ventricle wall and used to determine the position of aggregates (Fig. 2**, inset**). Cu K-edge spectra were recorded from aggregates. The resulting spectra from both MTKO and wild-type mice were very similar (Fig. 2) and displaying a form characteristic for the Cu(I) oxidation state and binding as a Cu_xS_y cluster [49].

3.3. Detection of orange-red optical fluorescence in subventricular zone

According to previous literature on Cu_xS_y clusters formed with biomolecules, they are expected to display fluorescence, a property of the electronic structure of Cu_xS_y cluster [45]. Fig. 3 shows optical images of the SVZ of mice brains obtained at room temperature with an excitation of 350 nm and emission detection at 550 nm. Along the lateral ventricle, orange-red emitting bodies are visible in fresh sections for WT (Fig. 3A) mice. MTKO mice also exhibit these bodies (Fig. 3B), but there is a noted decrease in the number of fluorescing spots along the ventricle wall. These results are in good agreement with XRF quantification of Cu-containing aggregates. As we have established that Cu aggregates are localized to astrocytes [53] we checked whether the lower number of Cu aggregates in MTKO could possibly be due to a lower density of astrocytes in this mutant. Staining of WT and MTKO mice for GFAP we did not detect any differences in the density of astrocytes in the SVZ (data not shown).

Knowing that Cu aggregates occur in astrocytes and that the detected optical fluorescence likely originates from Cu_xS_y clusters we co-localized the orange-red fluorescence with GFAP (Fig. 3D). The results show some clusters which co-localize strongly with GFAP (circles) and some which are adjacent to strong GFAP staining (arrows). We attribute the GFAP-adjacent clusters to being in weakly stained astrocyte processes, where XRF has previously shown some aggregates [53]. In accordance with our earlier finding that actively

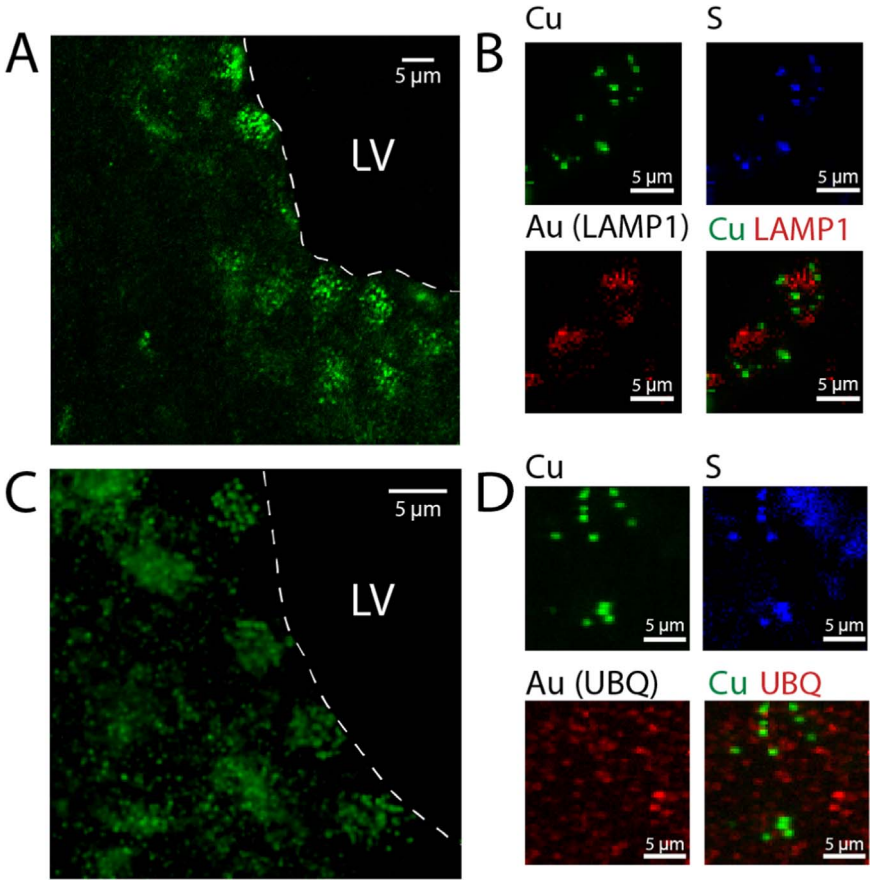

Fig. 4. Co-localization experiments for Cu inclusions with lysosomes (LAMP1) and ubiquitin (UBQ). **A.** Optical micrograph of staining for LAMP1 fluorescence showing that LAMP1 stains small puncta that reside mostly in cells. **B.** XRF co-localization of Cu (green), S (blue), and Au-labeled LAMP1 (red) showing that Cu does not reside in lysosomes in the SVZ. **C.** Optical micrograph showing ubiquitin fluorescence in the SVZ. Ubiquitin also forms small puncta that reside in cells. **D.** XRF co-localization of Cu (green), S (blue), and Au-labeled ubiquitin (red). These data show that Cu inclusions are not ubiquitinated. Data here are for a 9-week old mouse (A, B) and a 12-week old rat (C,D). (For interpretation of the references to color in this figure legend, the reader is referred to the web version of this article.)

dividing cell in the SVZ (a majority of which are migrating neuroblasts) are depleted of Cu aggregates we found that dividing cells labeled with a Ki67 marker do not contain fluorescing aggregates (Fig. 3C).

3.4. Immunohistochemical analyses of the SVZ

To test if Cu aggregates occur in typical degradation pathways, brain sections labeled for lysosomes (by LAMP1) or ubiquitin (UBQ) with Au nano-conjugated antibodies were XRF imaged, allowing co-localization of these biological markers with Cu. Au maps were formed using the Au L edge. To confirm staining was accurate, Au XRF maps were visually compared to optically stained sections (Fig. 4). It was found that Cu inclusions do not colocalize with LAMP1 (lysosomes) (Fig. 4B) and are not ubiquitinated (Fig. 4D), suggesting that the inclusions do not undergo autophagic process.

To assess the effect that the MTKO mutation has on neurogenic activity, we quantified Ki67, a marker for dividing cells in the SVZ. The cell density of Ki67+cells along the SVZ showed no significant difference between 9 week old WT (12.1 ± 1.2 cells/mm) and MTKO (12.9 ± 1.3 cells/mm) mice (Fig. 5). Stains for MT(1,2) were also carried out and no positive staining was observed in MTKO mice (Fig. 5,S4).

4. Discussion

MT(1,2) binds Cu or Zn and are, thus, involved with the homeostasis of these elements. Using quantitative XRF imaging on MTKO, we have not observed statistically significant changes in metal content in large brain areas such as striatum, corpus callosum, and cortex in spite of the well documented role of MT(1,2) in Cu and Zn homeostasis (Fig. 1A,Table 2). A possible explanation is that knockout of MT(1,2), expressed primarily in astrocytes, most drastically affects Cu accumulating astrocytes, which are present only in the subventricular zone for mice [66]. Among the identified regions, the only statistically significant difference was along the ventricle and only for Cu (Fig. 1B,Table 3). The SVZ, which has a high localized content of astrocytes, shows significant changes in the Cu content. High resolution imaging, which allows the visualization of individual aggregates (Fig. 1C) shows that this decrease is due to a decreased number of aggregates as well as decreased basal Cu in the SVZ. Aggregates which remain in MTKO mice, however, have comparable Cu concentrations as WT mice (Table 4). These results hint at the possibility of MT being directly involved with aggregate formation. Aggregates in both MTKO and wild-type mice had comparable [S]/[Cu] ratios.

A second suggestion of direct MT involvement with aggregates formation comes from observation of the autofluorescence. Here we expanded our characterization of the Cu-rich aggregates by demonstrating their orange-red optical fluorescence consistent with optical properties of Cu_xS_y clusters bound in a biological molecule (Fig. 3). It has been long known that, in mammalian cells, the majority of autofluorescence activity is derived from nicotinamide adenine dinucleotide (NADH) or riboflavins (or their flavin coenzymes) [39]. While both NADH [8] and flavin adenine nucleotide (FAD) [2] autofluorescence under UV excitation, neither maximum emission is above 550 nm, thereby ruling them out from orange-red emission reported here. The fact that fluorescence is detected at room temperature rules

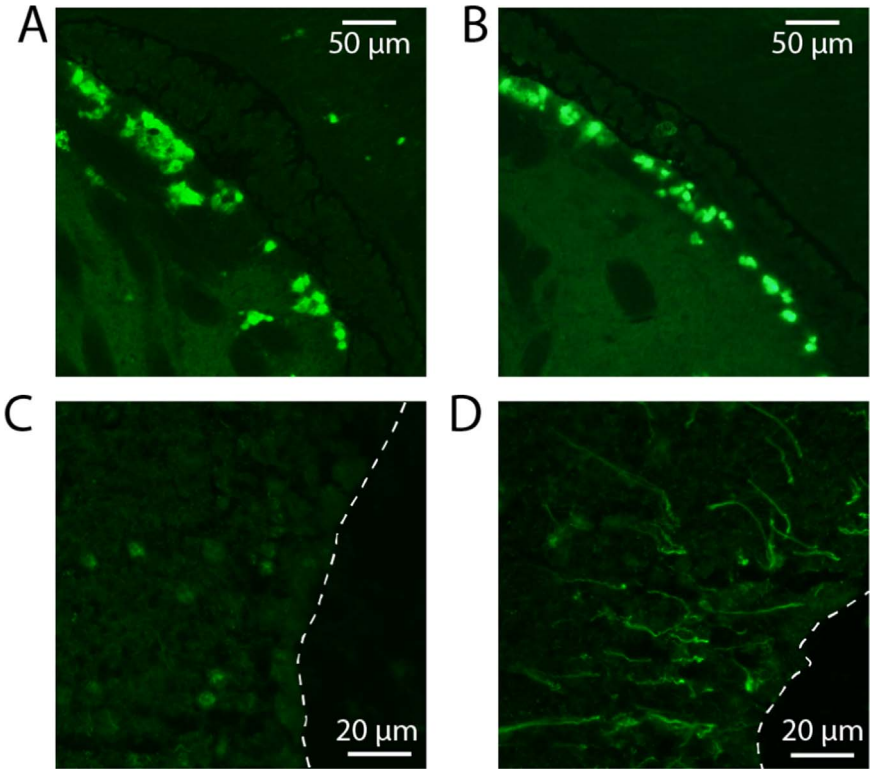

Fig. 5. Representative immunohistochemical stains for Ki67 for MTKO (A) and wild-type (B). Images like this along the entire ventricle were used for quantification of neurogenesis. Stains for MT(1,2) are shown for MTKO (C) and wild type (D). With the exception of a few negatively stained cell bodies (see SI), MTKO mice do not stain positively for MT(1,2) while wild-type mice show strong expression in the processes of astrocytes. Data are for 9-week old mice.

out the possibility that Cu is bound to low molecular weight compounds such as glutathione, which are known to fluoresce only at low temperature [14]. The reported autofluorescence clusters appear similar to those induced in the liver by $CuCl_2$ injection [65]. Rat brains for which we also have reported Cu aggregates show orange-red fluorescence from the SZV as well (data not shown). Here, we have presented substantial evidence suggesting that Cu aggregates detected by XRF fluorescence are the same as those detected by optical fluorescence including their similar co-localization with biological markers and a similar effect of MT knockout.

Cu-rich aggregates detected by XRF microscopy are similar to previously reported Gomori-positive inclusions (GPIs). GPIs are periventricular inclusion bodies that are characterized by their i) metal-rich composition, ii) localization to astrocytes, iii) orange-red autofluorescence, iv) ubiquitination, and v) non-enzymatic peroxidase activity [60]. GPIs may be related to corpora amylacea [61,62] and thus may be involved in the etiology of several diseases including Alzheimer's disease and epilepsy [16,35,44]. There are conflicting reports on whether GPIs are Cu- or Fe-rich [11,63], though we have demonstrated that both Cu- and Fe-rich aggregates are present in periventricular astrocytes and exhibit pseudoperoxidase activity [66]. One issue preventing a conclusive detailing of the metal-rich aggregates in periventricular astrocytes is that they have been studied in a variety of systems and under different experimental conditions, which makes direct comparisons challenging. GPIs induced by cysteamine exposure, for instance, were demonstrated to be immunoreactive to stress proteins including heat shock proteins and ubiquitin and to be Fe-rich [41]. Our current data demonstrates Cu-rich aggregates which are not immunoreactive to ubiquitin (Fig. 4) but are otherwise homologous to GPIs. Likely there is a critical difference between cysteamine-induced GPIs and naturally occurring aggregates. It was speculated, for instance, that GPIs form as a result of incompletely phagocytized mitochondria with putative assignment of peroxidase activity to some formed Fe-heme complex [10,62,63]. This formation mechanism is supported largely by experiments involving cysteamine-treated models. While this mechanism may hold some merit for Fe-rich, reportedly ubiquitinated aggregates in these astrocytes, it seems unlikely for Cu-rich aggregates, which our current evidence suggests is bound as a Cu_xS_y multimetallic cluster.

Protein aggregation is mainly counteracted by the cell in three fashions: increased refolding activity, lysosomal degradation, and proteosomal degradation by the ubiquitin-proteosome system (UPS). In order for proteins to be tagged for degradation via the UPS, they must be ubiquitinated. This data rules out the possibility that the inclusions are a part of aggresomes. Aggresomes are pericentrosomal, microtubule-dependent collections of misfolded proteins located in the endoplasmic reticulum [30,32]. The current data demonstrate that Cu-rich aggregates are not ubiquitinated (Fig. 4D), ruling out the notion that they are involved in proteasomal degradation. Furthermore, as we observe many inclusion bodies throughout astrocytes, including in the processes [53], it is clear that the Cu aggregates themselves are not aggresomes. In addition, no Cu-rich aggregates were found in lysosomes (Fig. 4B) nor were lysosomes found to have a higher Cu concentration than the surrounding regions as is expected if lysosomes responsible for phagocytosis of Cu-rich aggregates.

It is possible that decreased degradation to some extent causes Cu-rich aggregates to be toxic at advanced age. In human embryonic kidney cells, for instance, the presence of protein aggregates has been shown to compromise the UPS, either through interaction with the proteasome itself or an auxiliary protein [7]. The presence of aggregates then leads to a feedback loop in which individual proteins cannot be degraded quickly enough and thus can form additional aggregates which may not be immunologically active for ubiquitin. While cells are prone to protein aggregation when treated with proteasome inhibitor [26,33,5], cultured astrocytes in particular remain resilient due to their ability to upregulate macroautophagy under proteosomal stress [29]. While more-active macroautophagy protects cultured astrocytes, *in vivo* results suggest that advanced age comes with a diminished ability

to carry out macroautophagy [9]. With an impaired UPS and macroautophagy, older brains will be unable to correctly handle misfolded proteins, which may ultimately lead to neurodegeneration.

One critical finding of this study is that knocking out MT(1,2) did not completely eliminate Cu aggregates. (Fig. 1). There is a body of evidence suggesting that MT is required for formation of inclusions bodies. For instance, renal studies of Pb exposure found that while WT mice readily produce inclusion bodies in the kidney, likely as a means to mitigate damage from uptaken Pb, MTKO mice are unable to produce inclusion bodies under the same conditions [54] implicating MT as a necessary component for inclusion body formation. Furthermore, transfection of MT into MTKO cells recovered the ability to form inclusion bodies [76]. Plausibly, the persistence of aggregates in MTKO mice is due to the presence of MT3, which is expressed in the brain but not in the kidney [27,69].

While MT was originally found to be non-immunological in all Pb induced inclusions, a more extensive survey by the same group [73] found that around 16% of Pb-induced renal inclusions are strongly immunologically reactive with MT(1,2) while the majority (55.3%) remain immunonegative. Our stains for MT(1,2) have not turned up any puncta which are immunoreactive to MT(1,2) (Fig. 5,S4). There are several plausible explanations. It is possible that MT is not present in aggregates, in which case an MT-like protein must be binding Cu. If MT indeed is the binding protein, then aggregates may not immunoreactive to MT(1,2), as is the case for the majority of Pb-induced inclusions in the kidney. Alternatively, aggregates may be immunostained by MT(1,2) antibodies do not provide adequate contrast for detection since MT(1,2) strongly stains the cytoplasm of astrocytes (Fig. 5).

Quantitation of Ki67 showed no significant differences in neurogenic activity resulting from the MTKO mutation (Fig. 5,Table 4). The MTKO phenotype has been shown to be critical for repair following insults such as seizure and blunt force trauma [47] but to the best of our knowledge natural neurogenic rates in the SVZ have not been reported. In that light it is surprising that neurogenesis in the SVZ is unaffected. If Cu-rich aggregates play a role in neurogenesis, it is possible that their function is recovered by another mechanism.

Acknowledgements

We acknowledge the group of Dr. Wei Zheng from Purdue University's School of Health and Human Sciences for their help with animal handling and for Dr. Stefan Vogt for his help with the MAPS spectral fitting program. Use of the APS at ANL was supported by the U.S. Department of Energy, Office of Science, Office of Basic Energy Sciences, under Contract No. DE-AC02-06CH11357. The Biophysics Collaborative Access Team (BioCAT) is supported by grant P41 GM103622 from the National Institute of General Medical Sciences of the National Institutes of Health. PNC/XSD facilities at the Advanced Photon Source, and research at these facilities, are supported by the U.S. Department of Energy – Basic Energy Sciences, the Canadian Light Source and its funding partners, and the Advanced Photon Source. This study was supported by NIH/National Institute of Environmental Health Sciences Grants Numbers R01 ES008146-14, by Purdue start up funds and by NSF summer research experience for undergraduates program to J.O.

Appendix A. Supporting information

Supplementary data associated with this article can be found in the online version at doi:10.1016/j.redox.2016.12.007.

References

[1] N.J. Abbott, L. Ronnback, E. Hansson, Astrocyte-endothelial interactions at the blood-brain barrier, Nat. Rev. Neurosci. 7 (1) (2006) 41–53.
[2] J. Aubin, Autofluorescence of viable cultured mammalian cells, J. Histochem. Cytochem. 27 (1) (1979) 36–43.
[3] K.J. Barnham, A.I. Bush, Metals in alzheimer's and parkinson's diseases, Curr. Opin. Chem. Biol. 12 (2) (2008) 222–228.
[4] R. Barrea, D. Gore, E. Kondrashkina, T. Weng, R. Heurich, M. Vukonich, et al. The BioCAT microprobe for X-ray fluorescence imaging, MicroXAFS and microdiffraction studies on biological samples, in: Proceedings of the 8th International Conference on X-ray Microscopy IPAP Conference Series, 2006, pp. 230–232
[5] N.G. Bauer, C. Richter-Landsberg, The dynamic instability of microtubules is required for aggresome formation in oligodendroglial cells after proteolytic stress, J. Mol. Neurosci. 29 (2) (2006) 153–168.
[6] J.S. Becker, D. Salber, New mass spectrometric tools in brain research, TrAC Trends Anal. Chem. 29 (9) (2010) 966–979.
[7] N.F. Bence, R.M. Sampat, R.R. Kopito, Impairment of the ubiquitin-proteasome system by protein aggregation, Science 292 (5521) (2001) 1552–1555.
[8] R. Benson, R. Meyer, M. Zaruba, G. McKhann, Cellular autofluorescence–is it due to flavins?, J. Histochem. Cytochem. 27 (1) (1979) 44–48.
[9] E. Bergamini, G. Cavallini, A. Donati, Z. Gori, The role of macroautophagy in the ageing process, anti-ageing intervention and age-associated diseases, Int. J. Biochem. Cell Biol. 36 (12) (2004) 2392–2404.
[10] J.R. Brawer, G. Reichard, L. Small, H.M. Schipper, The origin and composition of peroxidase-positive granules in cysteamine-treated astrocytes in culture, Brain Res. 633 (1) (1994) 9–20.
[11] J.R. Brawer, R. Stein, L. Small, S. Cissé, H.M. Schipper, Composition of Gomori-positive inclusions in astrocytes of the hypothalamic arcuate nucleus, Anat. Rec. 240 (3) (1994) 407–415.
[12] P.C. Bull, G.R. Thomas, J.M. Rommens, J.R. Forbes, D.W. Cox, The wilson disease gene is a putative copper transporting P-type ATPase similar to the menkes gene, Nat. Genet. 5 (4) (1993) 327–337.
[13] A.I. Bush, Metals and neuroscience, Curr. Opin. Chem. Biol. 4 (2) (2000) 184–191.
[14] J. Byrd, R.M. Berger, D.R. McMillin, C.F. Wright, D. Hamer, D.R. Winge, Characterization of the copper-thiolate cluster in yeast metallothionein and two truncated mutants, J. Biol. Chem. 263 (14) (1988) 6688–6694.
[15] Z. Cai, B. Lai, W. Yun, I. McNulty, A. Khounsary, J. Maser, et al. Performance of a high-resolution X-ray microprobe at the advanced photon source. Synchrotron Radiation Instrumentation, 521, 2000, pp. 31–34.
[16] J. Cavanagh, Corpora-amylacea and the family of polyglucosan diseases, Brain Res. Rev. 29 (2) (1999) 265–295.
[17] R. Chung, A. West, A role for extracellular metallothioneins in CNS injury and repair, Neuroscience 123 (3) (2004) 595–599.
[18] P. Coyle, J.C. Philcox, L.C. Carey, A.M. Rofe, Metallothionein: the multipurpose protein, CMLS 59 (2002) 627–647.
[19] N. D'Ambrosi, L. Rossi, Copper at synapse: release, binding and modulation of neurotransmission, Neurochem. Int. 90 (2015) 36–45.
[20] K.M. Davies, D.J. Hare, S. Bohic, S.A. James, J.L. Billings, D.I. Finkelstein, et al., Comparative study of metal quantification in neurological tissue using laser ablation-inductively coupled plasma-mass spectrometry imaging and X-ray fluorescence microscopy, Anal. Chem. 87 (13) (2015) 6639–6645.
[21] R. Dringen, I.F. Scheiber, J.F. Mercer, Copper metabolism of astrocytes, Front. Aging Neurosci. (2013) 5.
[22] P. Faller, C. Hureau, O. Berthoumieu, Role of metal ions in the self-assembly of the alzheimer's amyloid-β peptide, Inorg. Chem. 52 (21) (2013) 12193–12206.
[23] E.D. Gaier, B.A. Eipper, R.E. Mains, Copper signaling in the mammalian nervous system: synaptic effects, J. Neurosci. Res. 91 (1) (2013) 2–19.
[24] G.N. George, J. Byrd, D.R. Winge, X-ray absorption studies of yeast copper metallothionein, J. Biol. Chem. 263 (17) (1988) 8199–8203.
[25] G.N. George, D. Winge, C.D. Stout, S.P. Cramer, X-ray absorption studies of the copper-beta domain of rat-liver metallothionein, J. Inorg. Biochem. 27 (3) (1986) 213–220.
[26] O. Goldbaum, M. Riedel, T. Stahnke, C. Richter-Landsberg. The Small Heat Shock Protein HSP25 Protects Astrocytes Against Stress Induced by Proteasomal Inhibition, Glia, 57, 14, 2009, pp. 1566–1577.
[27] I. Hozumi, M. Asanuma, M. Yamada, Y. Uchida, Metallothioneins and neurodegenerative diseases, J. Health Sci. Tokyo 50 (4) (2004) 323–331.
[28] I. Hozumi, J.S. Suzuki, H. Kanazawa, A. Hara, M. Saio, T. Inuzuka, et al., Metallothionein-3 is expressed in the brain and various peripheral organs of the rat, Neurosci. Lett. 438 (1) (2008) 54–58.
[29] S.B. Jänen, H. Chaachouay, C. Richter-Landsberg, Autophagy is activated by proteasomal inhibition and involved in aggresome clearance in cultured astrocytes, Glia 58 (14) (2010) 1766–1774.
[30] J.A. Johnston, C.L. Ward, R.R. Kopito, Aggresomes: a cellular response to misfolded proteins, J. Cell Biol. 143 (7) (1998) 1883–1898.
[31] L.S. Kau, D.J. Spirasolomon, J.E. Pennerhahn, K.O. Hodgson, E.I. Solomon, X-ray absorption-edge determination of the oxidation-state and coordination-number of copper - application to the type-3 site in rhus-vernicifera laccase and its reaction with oxygen, J. Am. Chem. Soc. 109 (21) (1987) 6433–6442.
[32] R.R. Kopito, Aggresomes, inclusion bodies and protein aggregation, Trends Cell Biol. 10 (12) (2000) 524–530.
[33] D.H. Lee, A.L. Goldberg, Proteasome inhibitors cause induction of heat shock proteins and trehalose, which together confer thermotolerance in saccharomyces cerevisiae, Mol. Cell. Biol. 18 (1) (1998) 30–38.
[34] Y. Leung, M. Pankhurst, S. Dunlop, S. Ray, J. Dittmann, E. Eaton, et al., Metallothionein induces a regenerative reactive astrocyte phenotype via JAK/STAT and RhoA signalling pathways, Exp. Neurol. 221 (1) (2010) 98–106.
[35] J. MacKenzie, The surgical pathology of epilepsy: a study of 40 cases, Neuropathol. Appl. Neurobiol. 17 (1991) 526.
[36] B.A. Masters, E.J. Kelly, C.J. Quaife, R.L. Brinster, R.D. Palmiter, Targeted

disruption of metallothionein I and II genes increases sensitivity to cadmium, Proc. Natl. Acad. Sci. 91 (2) (1994) 584–588.
[37] A. Matusch, L.S. Fenn, C. Depboylu, M. Klietz, S. Strohmer, J.A. McLean, et al., Combined elemental and biomolecular mass spectrometry imaging for probing the inventory of tissue at a micrometer scale, Anal. Chem. 84 (7) (2012) 3170–3178.
[38] Z. Mirzadeh, F.T. Merkle, M. Soriano-Navarro, J.M. Garcia-Verdugo, A. Alvarez-Buylla, Neural stem cells confer unique pinwheel architecture to the ventricular surface in neurogenic regions of the adult brain, Cell Stem Cell 3 (3) (2008) 265–278.
[39] M. Monici, Cell and tissue autofluorescence research and diagnostic applications, Biotechnol. Annu. Rev. 11 (2005) 227–256.
[40] D.M. Morgan, J. Dong, J. Jacob, K. Lu, R.P. Apkarian, P. Thiyagarajan, et al., Metal switch for amyloid formation: insight into the structure of the nucleus, J. Am. Chem. Soc. 124 (43) (2002) 12644–12645.
[41] M.B. Mydlarski, H.M. Schipper, Stress protein co-localization to autofluorescent astrocytic inclusions in situ and in cysteamine-treated glial cultures, Brain Res. 627 (1) (1993) 113–121.
[42] K. Nakajima, K. Suzuki, Immunochemical detection of metallothionein in brain, Neurochem. Int. 27 (1) (1995) 73–87.
[43] N. Nishimura, H. Nishimura, A. Ghaffar, C. Tohyama, Localization of metallothionein in the brain of rat and mouse, J. Histochem. Cytochem. 40 (2) (1992) 309–315.
[44] S. Nishio, T. Morioka, T. Kawamura, K. Fukui, H. Nonaka, M. Matsushima, Corpora amylacea repiace the hippocampal pyramidal cell layer in a patient with temporal lobe epilepsy, Epilepsia 42 (7) (2001) 960–962.
[45] M. Okabe, K. Nakayama, M. Kurasaki, F. Yamasaki, K. Aoyagi, O. Yamanoshita, et al., Direct visualization of copper-metallothionein in LEC rat kidneys: application of autofluorescence signal of copper-thiolate cluster, J. Histochem Cytochem 44 (8) (1996) 865–873.
[46] P.A. Pella, D.E. Newbury, E.B. Steel, D.H. Blackburn, Development of National Bureau of Standards thin glass films for X-ray fluorescence spectrometry, Anal. Chem. 58 (6) (1986) 1133–1137.
[47] M. Penkowa, Metallothioneins are multipurpose neuroprotectants during brain pathology, FEBS J. 273 (9) (2006) 1857–1870.
[48] M. Penkowa, M. Giralt, J. Camats, J. Hidalgo, Metallothionein 1+2 protect the CNS during neuroglial degeneration induced by 6-aminonicotinamide, J. Comp. Neurol. 444 (2) (2002) 174–189.
[49] I.J. Pickering, G.N. George, C.T. Dameron, B. Kurz, D.R. Winge, I.G. Dance, X-ray-absorption spectroscopy of cuprous thiolate clusters in proteins and model systems, J. Am. Chem. Soc. 115 (21) (1993) 9498–9505.
[50] J.R. Prohaska, Long-term functional consequences of malnutrition during brain development: copper, Nutrition 16 (7–8) (2000) 502–504.
[51] M.J. Pushie, I.J. Pickering, G.R. Martin, S. Tsutsui, F.R. Jirik, G.N. George, Prion protein expression level alters regional copper, iron and zinc content in the mouse brain, Metallomics 3 (2) (2011) 206–214.
[52] Y. Pushkar, Synchrotron X-ray fluorescent imaging and spectroscopy studies of the role of copper in the stem cell niche architecture of adult neural stem cells, Biophys. J. 98 (3, Supplement 1) (2010) (745a-a).
[53] Y. Pushkar, G. Robison, B. Sullivan, S.X. Fu, M. Kohne, W. Jiang, et al., Aging results in copper accumulations in glial fibrillary acidic protein-positive cells in the subventricular zone, Aging Cell 12 (5) (2013) 823–832.
[54] W. Qu, B.A. Diwan, J. Liu, R.A. Goyer, T. Dawson, J.L. Horton, et al., The metallothionein-null phenotype is associated with heightened sensitivity to lead toxicity and an inability to form inclusion bodies, Am. J. Pathol. 160 (3) (2002) 1047–1056.
[55] T.D. Rae, P.J. Schmidt, R.A. Pufahl, V.C. Culotta, T. V. O'Halloran, Undetectable intracellular free copper: the requirement of a copper chaperone for superoxide dismutase, Science 284 (5415) (1999) 805–808.
[56] S. Saalfeld, P. Tomancák, Automatic landmark correspondence detection for Image J, in: Proceedings of the Image J User and Developer Conference, 2008, pp. 128–133.
[57] I.F. Scheiber, R. Dringen, Astrocyte functions in the copper homeostasis of the brain, Neurochem. Int. 62 (5) (2013) 556–565.
[58] I.F. Scheiber, J.F.B. Mercer, R. Dringen, Copper accumulation by cultured astrocytes, Neurochem. Int. 56 (3) (2010) 451–460.
[59] I.F. Scheiber, M.M. Schmidt, R. Dringen, Copper export from cultured astrocytes, Neurochem. Int. 60 (3) (2012) 292–300.
[60] H.M. Schipper, Gomori-positive astrocytes: biological properties and implications for neurologic and neuroendocrine disorders, Glia 4 (4) (1991) 365–377.
[61] H.M. Schipper, Experimental induction of corpora amylacea in adult rat brain, Microsc. Res. Tech. 43 (1) (1998) 43–48.
[62] H.M. Schipper, S. Cissé, Mitochondrial constituents of corpora amylacea and autofluorescent astrocytic inclusions in senescent human brain, Glia 14 (1) (1995) 55–64.
[63] H.M. Schipper, R. Vininsky, R. Brull, L. Small, J.R. Brawer, Astrocyte mitochondria: a substrate for iron deposition in the aging rat substantia nigra, Exp. Neurol. 152 (2) (1998) 188–196.
[64] M.L. Schlief, J.D. Gitlin, Copper homeostasis in the CNS, Mol. Neurobiol. 33 (2006) 81–90.
[65] M.J. Stillman, Z. Gasyna, A.J. Zelazowski, A luminescence probe for metallothionein in liver tissue: emission intensity measured directly from copper metallothionein induced in rat liver, FEBS Lett. 257 (2) (1989) 283–286.
[66] B. Sullivan, G. Robison, Y. Pushkar, J.K. Young, K.F. Manaye, Copper accumulation in rodent brain astrocytes: a species difference, J. Trace Elem. Med. Biol. 39 (2017) 6–13.
[67] M. Tavazoie, L. Van der Veken, V. Silva-Vargas, M. Louissaint, L. Colonna, B. Zaidi, et al., A specialized vascular niche for adult neural stem cells, Cell Stem Cell 3 (3) (2008) 279–288.
[68] E. Tiffany-Castiglioni, Y. Qian, Astroglia as metal depots: molecular mechanisms for metal accumulation, storage and release, Neurotoxicology 22 (5) (2001) 577–592.
[69] Y. Uchida, K. Takio, K. Titani, Y. Ihara, M. Tomonaga, The growth inhibitory factor that is deficient in the Alzheimer's disease brain is a 68 amino acid metallothionein-like protein, Neuron 7 (2) (1991) 337–347.
[70] M. van Lookeren Campagne, H. Thibodeaux, N. van Bruggen, B. Cairns, R. Gerlai, J.T. Palmer, et al., Evidence for a protective role of metallothionein-1 in focal cerebral ischemia, Proc. Natl. Acad. Sci. 96 (22) (1999) 12870–12875.
[71] S. Vogt, MAPS: a set of software tools for analysis and visualization of 3D X-ray fluorescence data sets, J. Phys. IV 104 (2003) 635–638.
[72] C. Vulpe, B. Levinson, S. Whitney, S. Packman, J. Gitschier, Isolation of a candidate gene for Menkes disease and evidence that it encodes a copper-transporting ATPase, Nat. Genet. 3 (1) (1993) 7–13.
[73] M.P. Waalkes, J. Liu, R.A. Goyer, B.A. Diwan, Metallothionein-I/II double knockout mice are hypersensitive to, Cancer Res. 64 (21) (2004) 7766–7772.
[74] M. Yamada, S. Hayashi, I. Hozumi, T. Inuzuka, S. Tsuji, H. Takahashi, Subcellular localization of growth inhibitory factor in rat brain: light and electron microscopic immunohistochemical studies, Brain Res. 735 (2) (1996) 257–264.
[75] J.K. Young, J.S. Garvey, P.C. Huang, Glial immunoreactivity for metallothionein in the rat brain, Glia 946 (1991) 602–610.
[76] P. Zuo, W. Qu, R.N. Cooper, R.A. Goyer, B.A. Diwan, M.P. Waalkes, Potential role of α-synuclein and metallothionein in lead-induced inclusion body formation, Toxicol. Sci. 111 (1) (2009) 100–108.